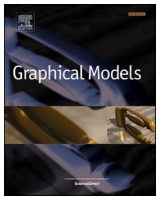
Graphical Models 139 (2025) 101263



Contents lists available at ScienceDirect

Graphical Models

journal homepage: www.elsevier.com/locate/gmod





An efficient parametric modeling and path planning method for 3D printing of curved surface corrugated sandwich structures

Tan Gui [a], Zhihong Li [b], Yongjun Cao [a], Jianghong Yang [a], Yingjun Wang [a,*]

[a] National Engineering Research Center of Novel Equipment for Polymer Processing, The Key Laboratory of Poly-mer Processing Engineering of the Ministry of Education, Guangdong Provincial Key Laboratory of Technique and Equipment for Macromolecular Advanced Manufacturing, South China University of Technology, Guangzhou 510641, China

[b] Shenzhen Piocreat 3d Technology Co. Ltd, Shenzhen 518110, China

ARTICLE INFO

Keywords:
Curved corrugated sandwich structures
Automatic modeling
FDM
Path planning
Compression testing

ABSTRACT

This study proposes an efficient preprocessing method and parametric modeling technique for the path planning of corrugated curved surface sandwich structures. Focusing on the characteristics of Fused Deposition Modeling (FDM), the model undergoes preprocessing for two types of path planning, segmenting the sandwich structure for Eulerian Path Printing (EPP) and Eulerian Circuit Printing (ECP). Algorithms were developed using the SolidWorks API for secondary development, resulting in a standalone plugin module. This plugin streamlines adaptive modeling of corrugated sandwich structures on curved surfaces, showcasing strong versatility. Additionally, a comparison of the printing time between preprocessed models and standard models reveals a significant reduction in nozzle idle time. Moreover, as the infill density increases, the reduction in printing time becomes more pronounced. Finally, compression tests confirmed that printed parts obtained using the EPP and ECP methods maintained comparable mechanical properties to those printed using conventional methods.

1. Introduction

The lightweight sandwich structure comprises upper and lower layer plates sandwiching an intermediate core, typically fabricated from metal, plastic, or composite materials [1,2]. As shown in Fig. 1, this structure can be categorized into random and periodic classes. Random types commonly employ foam or composite materials as fillers, serving purposes such as sound insulation and noise reduction [3]. The periodic class encompasses two-dimensional lattice [4–6] (The main focus of this article is the study of corrugated sandwich structures), three-dimensional lattice, and honeycomb structures [7,8] corrugated sandwich structures typically exhibit lower load-carrying capacities compared to honeycomb and three-dimensional lattice structures. However, when the upper and lower layers of a lightweight sandwich structure are curved, honeycomb structures are more susceptible to non-linear behavior. In such scenarios, corrugated sandwich structures offer distinct advantages [9,10]. Corrugated sandwich structures are widely utilized to enhance structural support and durability, notably in diverse applications ranging from civil engineering and bridge construction to aerospace, particularly for aircraft fuselage assemblies [11–13]. Common manufacturing techniques for corrugated sandwich structures encompass extrusion [14], stamping, and rolling processes [15]. The common feature among these methodologies is extrusion forming, particularly conducive to fabricating sandwich structures characterized by flat upper and lower surfaces. Nonetheless, due to the fixed-cycle nature of extrusion shaping, conventional sandwich manufacturing methods are unsuitable for curved sandwich configurations. Consequently, variations in sandwich height arise with the curvature of the surface, posing a challenge to traditional manufacturing processes.

Additive manufacturing, colloquially referred as 3D printing, represents a departure from conventional manufacturing paradigms, converting digital 3D models into tangible objects through the sequential deposition of materials layer by layer [16]. Common additive manufacturing techniques encompass Selective Laser Melting (SLM) [17], Selective Laser Sintering (SLS), and Fused Deposition Modeling (FDM).

Currently, FDM stands out as the predominant process due to its versatility in utilizing diverse materials and its capacity to consistently and reliably fabricate functional objects and components [18,19].Additive manufacturing offers significant advantages in its capacity to fabricate intricate models, yet its layer-by-layer approach often results

* Corresponding author.
E-mail address: wangyj84@scut.edu.cn (Y. Wang).

https://doi.org/10.1016/j.gmod.2025.101263
Received 31 October 2024; Received in revised form 31 March 2025; Accepted 1 April 2025
Available online 10 April 2025
1524-0703/© 2025 The Author(s). Published by Elsevier Inc. This is an open access article under the CC BY-NC license (http://creativecommons.org/licenses/by-nc/4.0/).

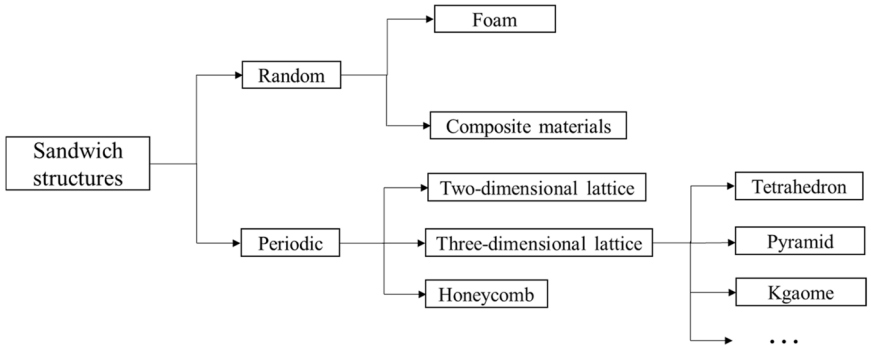


Fig. 1. Classification of sandwich structures.

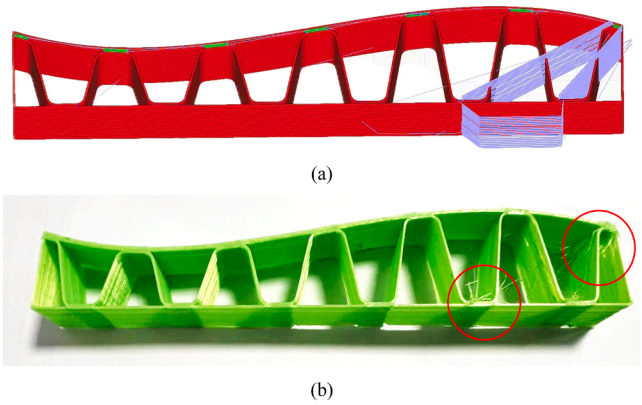


Fig. 2. Direct printing of corrugated sandwich structures: (a) Ultimaker Cura slicing preview visualization, (b) The printed parts exhibiting stringing phenomena.

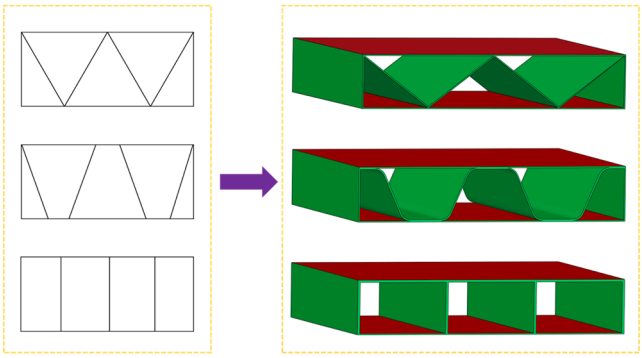
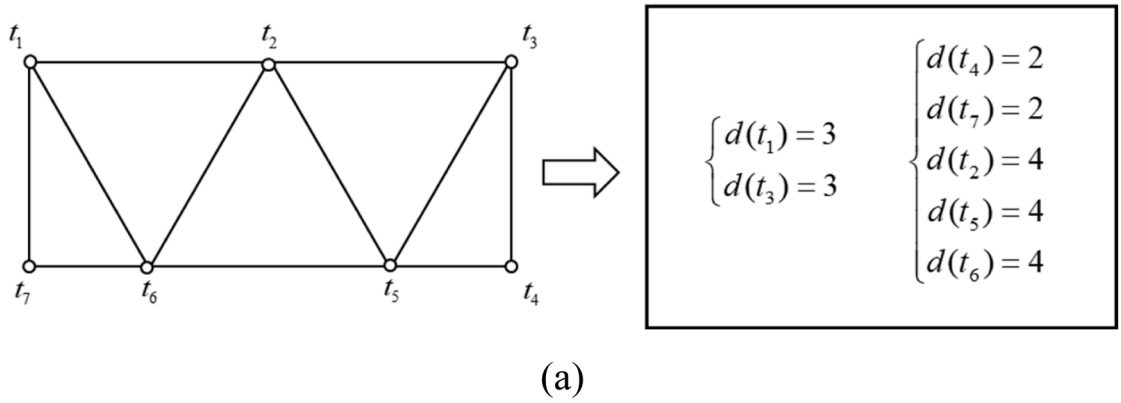


Fig. 3. Three types of infill patterns: triangular, trapezoidal, and cap-shaped.

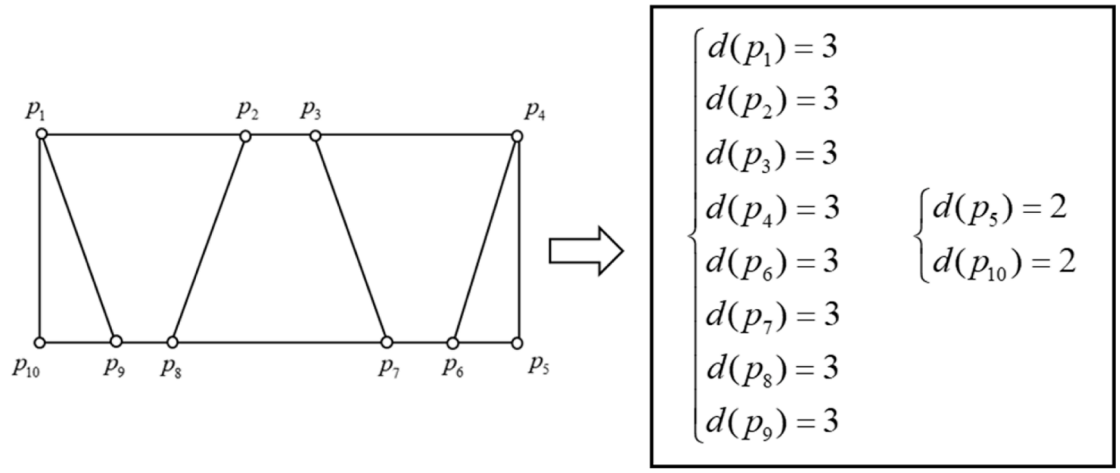
in slower production than anticipated. Researchers, such as Han et al. [20], underscored the importance of reducing additive manufacturing time through deposition planning methods employing grouping and mapping algorithms. In FDM printing, inherent nozzle start-stop actions during idle travel are inevitable, making strategic path planning crucial for enhancing both efficiency and quality [21]. Yamamoto et al. [22] have developed a single-trip path visualization Euler diagram for continuous printing based on the constrained Hierholzer algorithm. TU and collaborators [23] have introduced a shearing method and corresponding device to facilitate multiple cuts at intersection points, thereby enabling continuous printing paths. However, current research mainly focuses on path planning for the filling of solid models, with little related research on the corrugated sandwich structure itself. This study does not require complex path planning algorithms for computation. Instead, it achieves printing using ECP and EPP path methods through model slicing and preprocessing, thereby improving the printing efficiency and quality of curved corrugated sandwich structures. This approach enables direct G-code generation via slicing software, thereby streamlining the printing process.

Bates et al. [24] showcased the considerable potential of FDM 3D printing for fabricating sandwich structures, emphasizing their energy absorption capabilities. Concurrently, Chen et al. [25] conducted experiments on FDM-printed honeycomb layered structures to assess their compressive strength. Rajpa et al. [26] investigated the physical properties of various filling shapes positioned at different angles, employing 3D printing techniques with varied parameters. Additionally, Sabah Pirouzfar and colleagues [27] used FDM printing technology to study the impact of different geometric parameters on the bending performance of 3D printed honeycomb structures. While previous studies predominantly focused on planar upper and lower layers in lightweight sandwich structures, real-world applications often involve curved surfaces. In the aforementioned study, the research focuses on planar upper and lower panels of lightweight sandwich structures [28]. In practical engineering applications, however, these panels are predominantly curved, such as those used in wind turbine blades [29] and various architectural fields [30,31]. Modeling lightweight sandwich structures with curved panels presents greater complexity, requiring time-consuming and less efficient preprocessing for modeling.

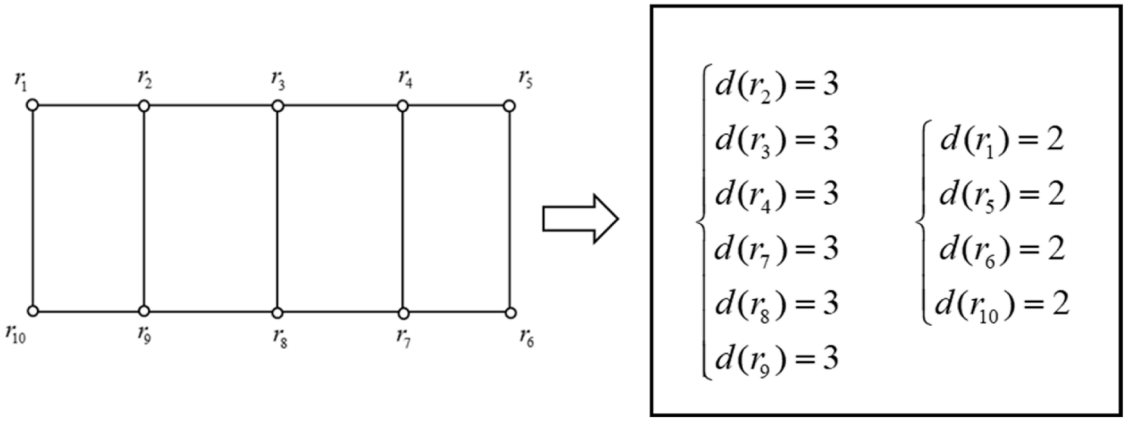
Parametric modeling encompasses the swift generation of 3D models and the execution of parametric simulation analyses utilizing CAD/CAE software. Through the precise definition and management of parameter variables, this methodology enables efficient construction and modification of model designs. Manipulating these parameters facilitates adjustments in dimensions, geometric configurations, or analytical parameters, thereby accommodating diverse requirements in design and analysis tasks. This research centers on parametric modeling within SolidWorks, specifically targeting the efficient development of a curved corrugated sandwich structure optimized for direct application in 3D printing processes. Researchers such as Danjou et al. [32] have leveraged the SolidWorks API to develop CAD systems for specialized tasks based on Knowledge-Based Engineering (KBE). Shaqura et al. [33] have devised an automated CAD modeling software system for multi-rotor micro Unmanned Aerial Vehicles (UAVs) using the SolidWorks API. Meanwhile, Yang et al. [34] have implemented 3D fracture geometric visualization of directional wells by undertaking secondary development of SolidWorks. Such initiatives contribute to understanding fracture orientation and distortion characteristics during fracturing operations, crucial for optimizing fracturing design. Zhang et al. [6] utilized ABAQUS/Explicit with custom-developed user parameterized modeling scripts to analyze the impact of varying corrugation angles and operating conditions on the mechanical performance of corrugated sandwich structures. However, there exists a gap in research concerning automated parametric modeling of lightweight sandwich structures, particularly curved ones. These structures exhibit high modeling



(a)



(b)



(c)

Fig. 4. Three types of infill patterns and their vertex degrees: (a) Triangular (b) Trapezoidal,(c) Cap-shaped.

complexity, often necessitating laborious modeling processes. This paper addresses this gap by developing a plugin interface system based on SolidWorks for adaptive parametric automatic modeling of various curved surfaces. In this paper's automatic modeling process, the lightweight sandwich structure model undergoes preprocessing with slits to aid subsequent 3D printing path planning. This approach aims to minimize nozzle idle travel during printing, thereby reducing printing time and enhancing printing efficiency and quality.

This study developed an automated modeling plugin based on SolidWorks to efficiently and with high quality perform parametric modeling of lightweight sandwich structures with curved surfaces. The design includes Euler path and Euler circuit planning for three types of fill configurations: triangular, corrugated, and cap-shaped. The model undergoes preprocessing for seam cutting prior to 3D printing, facilitating direct application in the printing process to reduce printing time and enhance overall efficiency and quality. This study fills the research

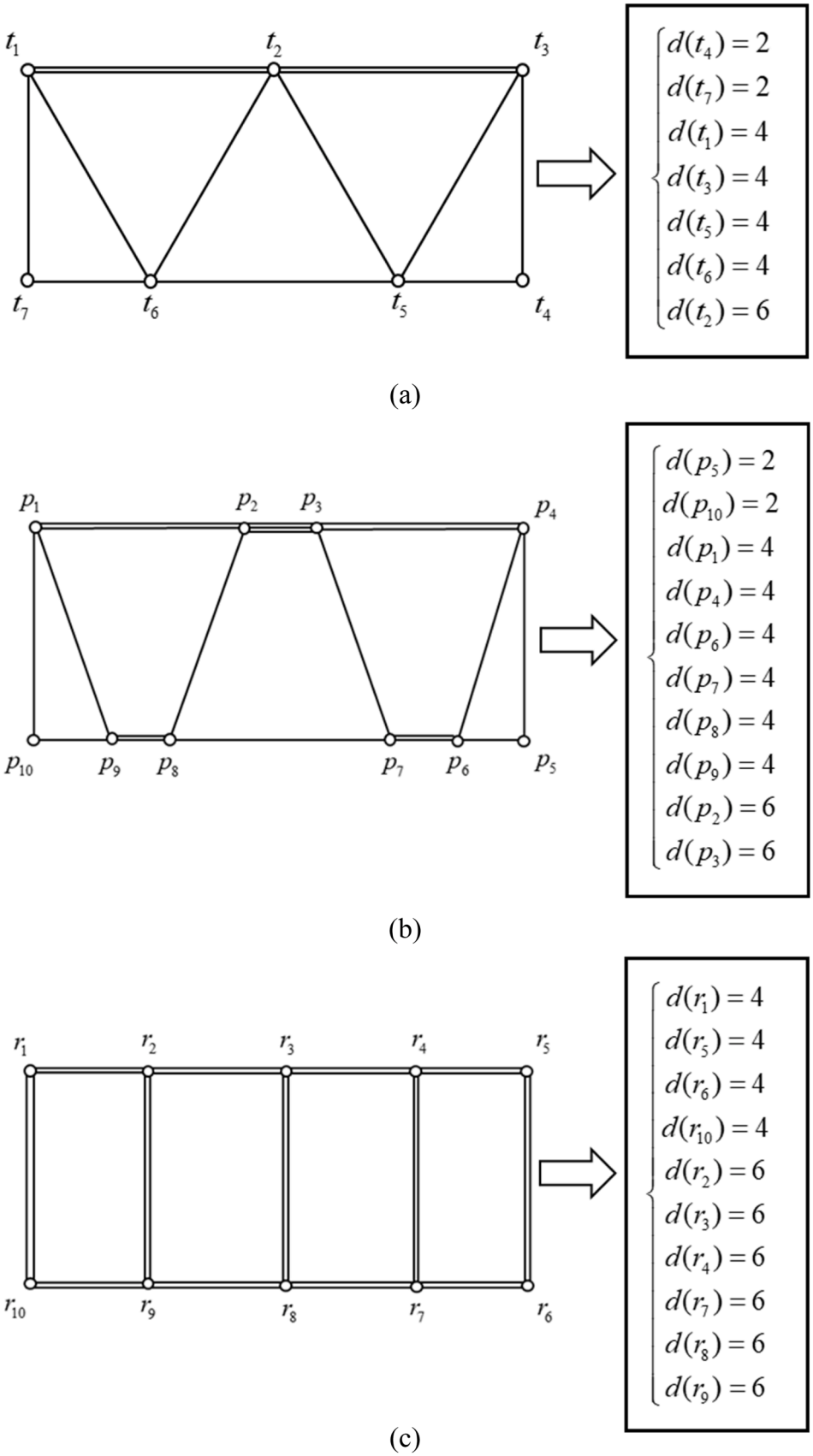


Fig. 5. Three types of infill structures after altering the path planning: (a) Triangular (b) Trapezoidal,(c) Cap-shaped.

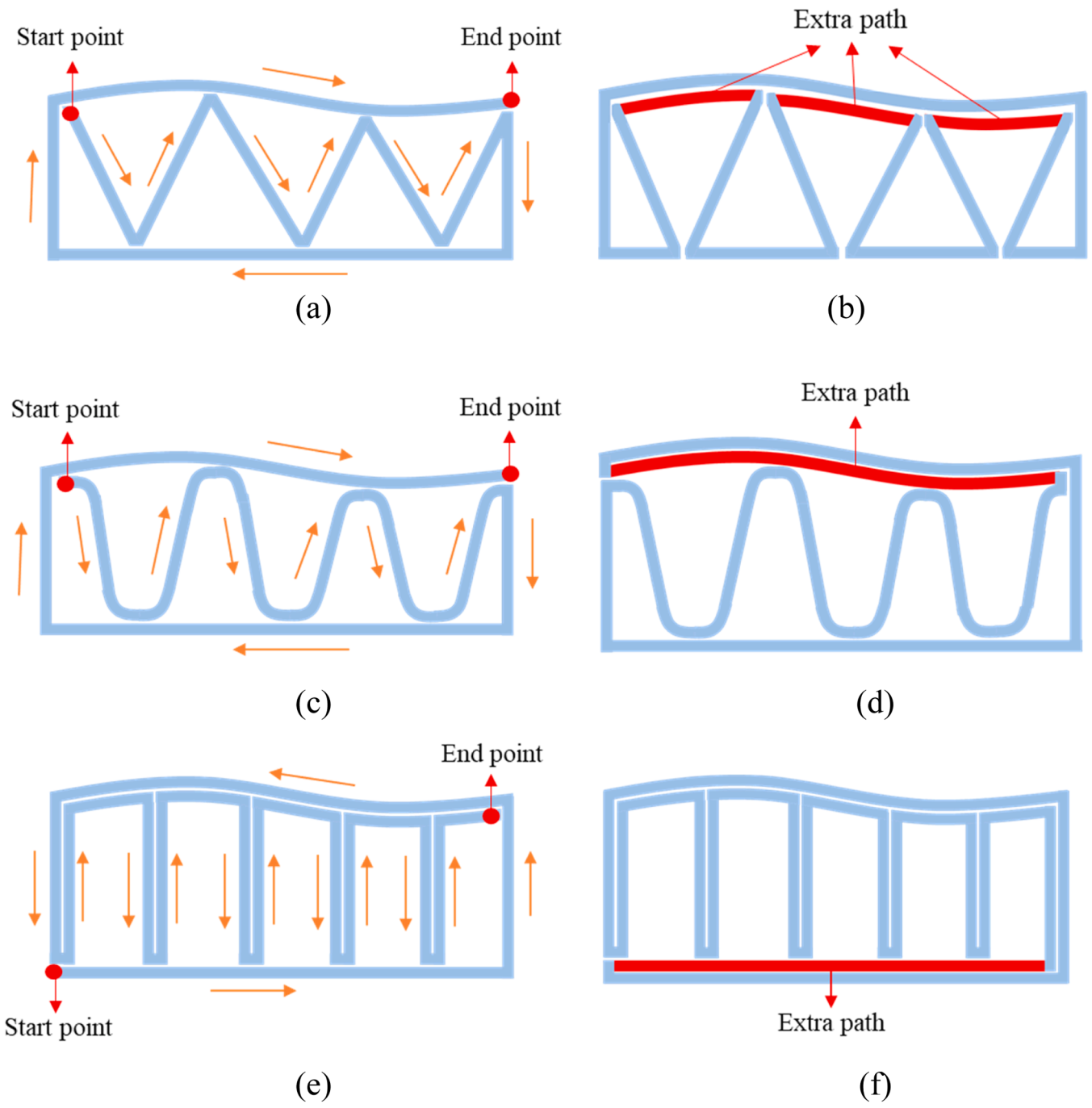


Fig. 6. Six schematic diagrams of printing paths: (a) Triangular EPP infill (b) Triangular ECP infill (c) Trapezoidal EPP infill (d) Trapezoidal ECP infill (e) Cap-shaped EPP infill (f) Cap-shaped ECP infill.

gap in path planning for additive manufacturing of curved corrugated sandwich structures. Without relying on complex path planning algorithms, it directly preprocesses the model to achieve efficient and rational printing paths. Additionally, it offers adaptability to various irregular surfaces and addresses the challenges of curved surface modeling through parametric modeling. The subsequent sections of this paper are structured as follows: Section 2 explores the design of the path planning method for curved sandwich structures; Section 3 outlines the parametric modeling approach for curved sandwich structures using SolidWorks; Section 4 analyzes the printing time and conducts mechanical performance testing of the corrugated sandwich structure; Section 5 concludes the paper.

2. Euler path and Euler circuit method

2.1. D printing path methods

FDM is a prevalent 3D printing technology that constructs three-dimensional objects by extruding material through a nozzle and layering it sequentially. The printer's operations are typically governed by G-code files, which are programming language instructions specifying nozzle control, heating parameters, speed, and retraction settings. Due to the modifiable properties of G-code files, many researchers have used algorithms to modify G-code files for printhead path planning. For example, Yuan Jin [35,36] developed several applications for FDM filling path planning using the CGAL *C++* library, including planning

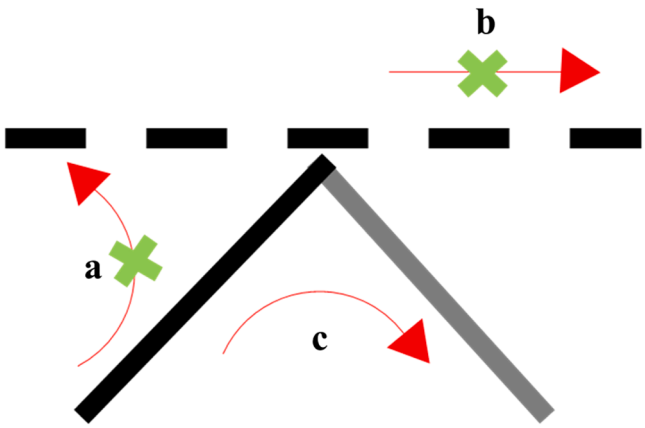


Fig. 7. Illustration of seam cutting paths.

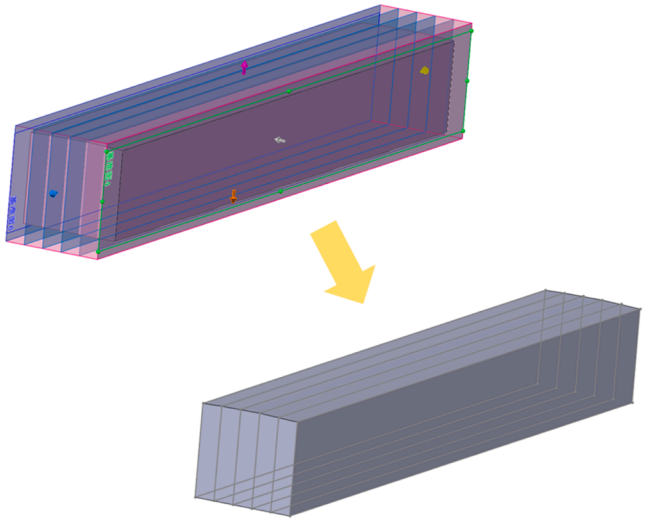


Fig. 8. Model slicing in SolidWorks.

corrugated paths for thin-walled structures. While previous studies primarily focus on modifying G-code using complex path planning algorithms, research on path planning for inherently corrugated sandwich structures remains scarce. In contrast, this study utilizes adaptive parametric geometric modeling to achieve 3D printing path planning, significantly enhancing the modeling and printing efficiency of curved corrugated sandwich structures. Building on the concept of corrugated sandwich structures, this paper directly generates a printable corrugated sandwich model tailored to user requirements from a given surface CAD model.

In traditional workflows, 3D printing slicing software such as Ultimaker Cura, PrusaSlicer, and Simplify3D is used for path planning and generating G-code files. These paths often include significant idle travel, as depicted in Fig. 2(a), a preview from Ultimaker Cura showing light purple lines indicating nozzle idle travel in simulating a curved corrugated sandwich structure. Such idle travel can result in inefficient printing times and impact print success rates. Improper adjustment of filament retraction speed, distance, and nozzle temperature before printing can lead to stringing issues, as illustrated in Fig. 2(b). This phenomenon is evident in the fine strings left on parts of the conventional curved corrugated sandwich structure due to inadequate retraction control. These strings severely compromise the strength and surface quality of the printed components.

Therefore, effective path planning is a critical aspect of the FDM printing method. It involves optimizing the nozzle's movement path during printing to enhance both efficiency and quality. Euler graphs are frequently employed in path planning, encompassing Euler paths$G(V,E)$ and Euler circuits$G_\varepsilon(V,E_\varepsilon)$.

An Euler path$G(V,E)$ is a trail in a graph that visits every edge exactly once and has exactly two vertices of odd degree $d(v_i)$, serving as the start and end points. This path allows traversal through each edge without repetition, utilizing the two odd-degree vertices as endpoints. An Euler circuit$G_\varepsilon(V,E_\varepsilon)$, on the other hand, is a type of Euler path$G(V,E)$ that starts and concludes at the same vertex, thus forming a closed loop. In an Euler circuit$G_\varepsilon(V,E_\varepsilon)$, all vertices exhibit an even degree. To transform an Euler path$G(V,E)$ into an Euler circuit$G_\varepsilon(V,E_\varepsilon)$, additional edges W are added to eliminate the odd-degree vertices[37].

2.2. The path design of corrugated sandwich structures

Common types of corrugated sandwich structures include triangular, trapezoidal, and cap-shaped designs[38], as shown in the Fig. 3. To reduce stress concentration at the four vertices of the trapezoidal fill pattern, the corners are filleted, which does not affect the printing paths.

To find a reasonable Euler path and Euler circuit in the three types of fillings, the vertices in the simplified diagram are numbered as shown in the Fig. 4. In the triangular filling, there are two vertices with odd degrees, and in the trapezoidal and cap-shaped fillings, there are eight and six vertices with odd degrees respectively. Therefore, the corrugated sandwich structured core of the triangular filling is exactly an Euler path, but not an Euler circuit, while the corrugated sandwich structured cores of the trapezoidal and cap-shaped fillings are neither Euler paths nor Euler circuits.

Drawing inspiration from Hierholzer's Algorithm [39], an Euler circuit is formed when all vertices in a path graph possess even degrees. Among the three types of infill patterns, a set of edges W is introduced to ensure all vertex degrees become even, as illustrated in the Fig. 5.

For triangular infill, depicted in the Fig. 5(a), a path is added between t_1 and t_2, and between t_2 and t_3 to resolve the odd-degree vertices t_1 and t_3.In the case of trapezoidal infill, as shown in the Fig. 5(b), paths are added between p_1 and p_2, p_3 and p_4, p_6 and p_7, p_8 and p_9, and two paths are added between p_2 and p_3 to address the odd-degree vertices p_1 and p_4.For cap-shaped infill, shown in the Fig. 5(c), paths are simply added between each pair of adjacent vertices to ensure all vertices achieve even degrees.

Based on the schematic diagrams of the paths described above, six printing paths can be derived as shown in the Fig. 6. Under the Euler path printing (EPP) mode, the print head initiates extrusion at the origin and traverses uniformly towards the terminus in accordance with the directional arrows, as shown in Fig. 4(a), (c), and (e). Conversely, in the Euler circuit printing (ECP) mode, the initial position of the print head is arbitrary, returning to the original starting point after each layer without necessitating adjustments to filament retraction parameters. This optimization minimizes the duration spent on the print head's idle traversal. However, as illustrated in Fig. 4(b), (d), and (f), conforming to the requirements of ECP entails an additional layer of printing path compared to the EPP, resulting in increased material consumption and prolonged printing times. Hence, for distinct practical scenarios, a judicious selection of printing method is warranted.

3. Parametric modeling

In practical engineering applications, modeling curved corrugated sandwich structures involves a complex and meticulous process. Traditional methods struggle with the varying heights of each layer in the corrugated structure, requiring separate construction of each support cycle, thus intensifying modeling challenges. Furthermore, addressing diverse engineering requirements necessitates managing numerous variable parameters.

To address these challenges, this study undertakes GUI-based secondary development using SolidWorks to develop a plugin for

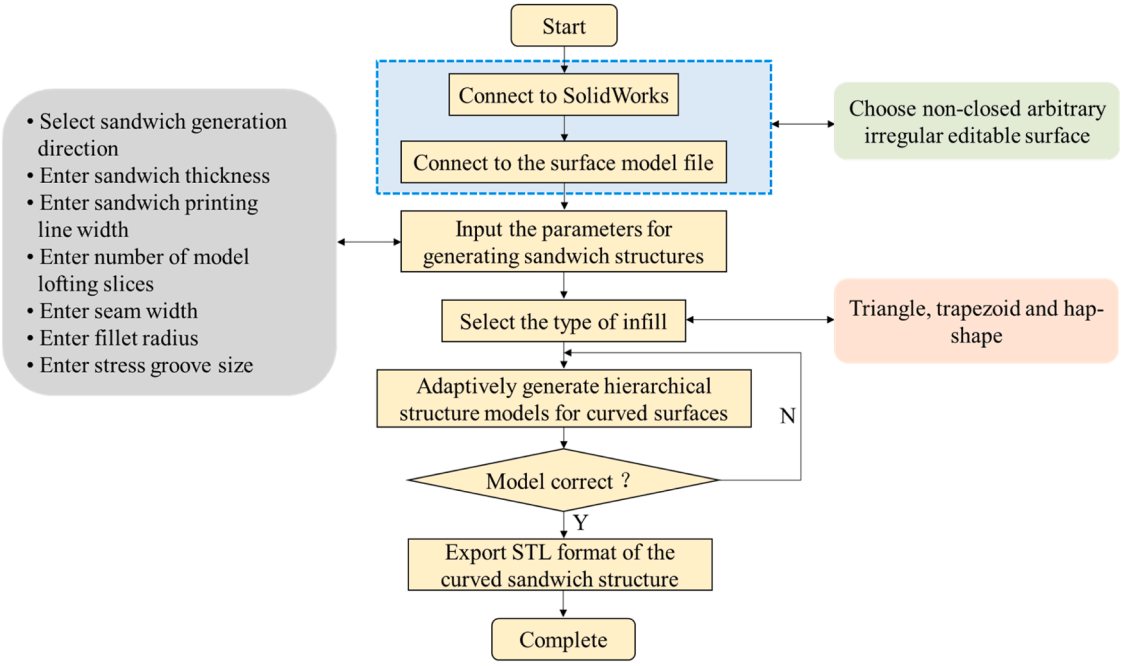


Fig. 9. Flowchart of system development.

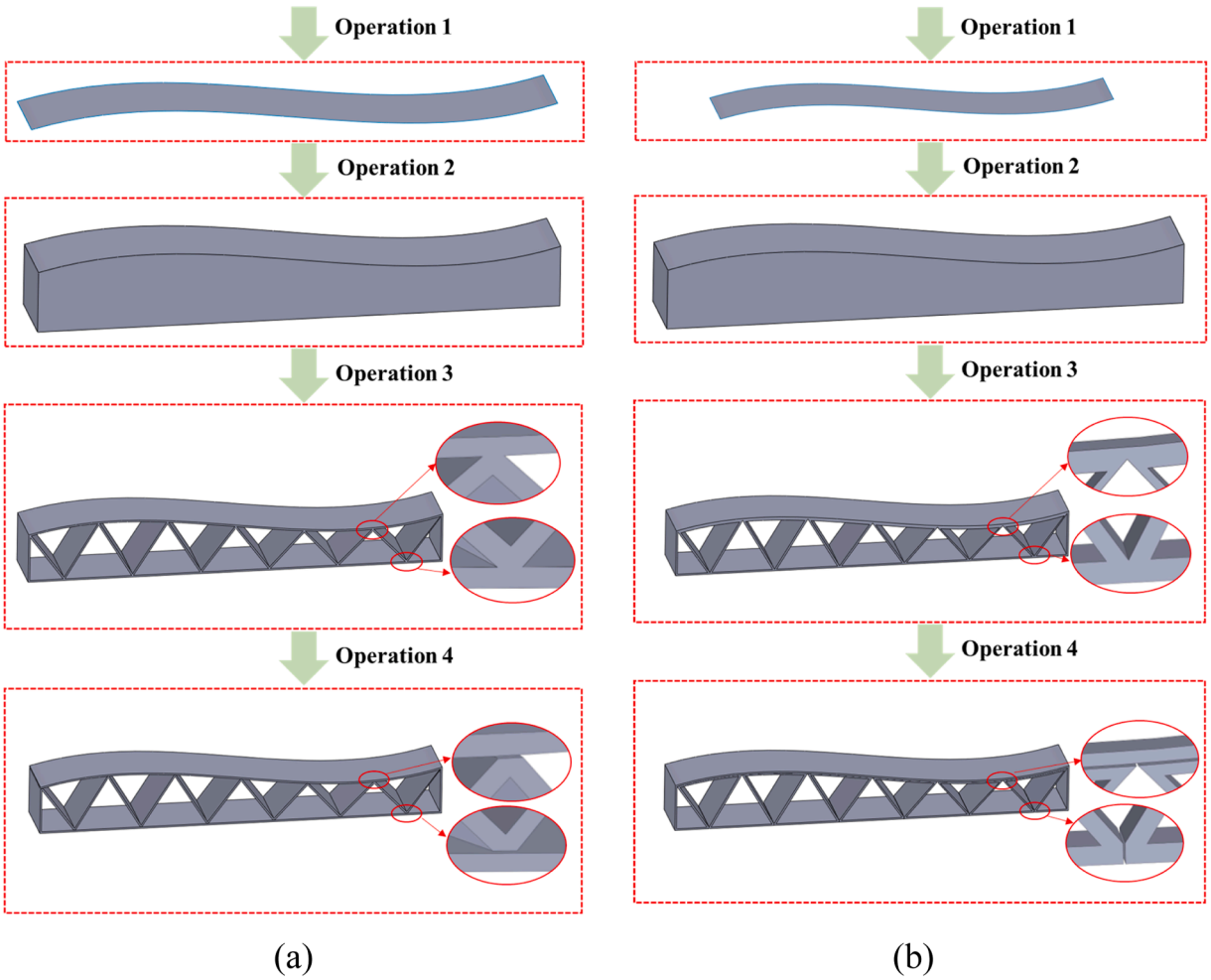


Fig. 10. Automated modeling process: (a) EPP method (b) ECP method.

Table 1
Sketch construction and Lofting.

```
Algorithm 1
1: Input: FillType, SliceNum
    // The filling types include triangular, trapezoidal, and cap-shaped.
2:    boolstatus = swmodel.Extension.SelectByID2(SliceRefPlaneArray(i), "PLANE", 0, 0, 0,
3:    True, 0, Nothing, 0)
4:    swmodel.SketchManager.InsertSketch True
5:    Set swsketch11 = swmodel.SketchManager.ActiveSketch
    // Drawing Closed Polygons Using Clipping Method.
6: For each edge=GetEdges(FillType) do
7:    status = long_line(swapp, swmodel, point2, point3, mul1, mul2, False, point_3,point_4,
8:    line_name2)
9:      If EdgeNum=GetEdgesNum(FillType) Then
10:       For i = 0 To EdgeNum
11:         boolstatus = swmodel.SketchManager.SketchTrim(0, off_point(0), off_point(1), 0)
12:       Next i
13:     End if
14: Next
    // Loft Cut.
15: Do While (Loft is not nothing)
16:    For k = 0 To Slicenum - 1
17:       boolstatus = swmodel.Extension.SelectByID2(sketchname1(k), "SKETCH",
18:       rec_loft(k)(0), rec_loft (k)(1), rec_loft (k)(2), True, 1, Nothing, 0)
19: Next k
20: Set Loft = swmodel.FeatureManager.InsertCutBlend(False, True, False, 1, 0, 0, False, 0, 0, 0, True, True)
21: Wend
```

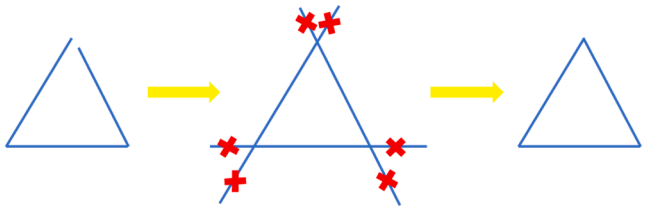


Fig. 11. Clipping method diagram.

parametric modeling of 3D models of curved corrugated sandwich structures. Detailed program steps and model construction have been outlined, and parameters for adaptive construction have been defined. In SolidWorks, most modeling operations can be facilitated through macro recording, aligning with API commands provided by SolidWorks encompassing properties, objects, and functions. Macro recording streamlines the exploration of SolidWorks' API interfaces, reducing development complexity and enhancing efficiency.

Current research in additive manufacturing path planning focuses on algorithm development integrated within slicing software, which controls nozzle trajectories through exported G-code files. This study innovates by planning printing paths directly from the 3D model design stage, facilitating STL model output for subsequent path planning in slicing software. This approach ensures compliance with EPP or ECP requirements.

During the modeling process, seams are strategically cut in the model, creating narrow gaps between paths in different directions. Slicing software utilizes these gaps to determine optimal printing directions, illustrated in the Fig.7. where path "c" is selected by the nozzle. The narrow gaps typically measure within 0.1 mm in the three-dimensional model, ensuring during FDM printing that material melting characteristics promote bonding without separation between core fill and upper/lower layers.

In slicing software, the slicing operation entails the systematic decomposition of a three-dimensional model into a succession of planar layers, commonly referred to as slices, facilitating the incremental construction of the object by the 3D printer. This process involves the conversion of the three-dimensional model into a sequence of two-dimensional images, each corresponding to a horizontal cross-section to be printed. Subsequently, these slices are sequentially transmitted to the 3D printer and incrementally assembled layer by layer to realize the ultimate three-dimensional object. However, the slicing mentioned in this section is different; the slicing referred to here is the slicing function in SolidWorks. The slicing function in SolidWorks is typically used to create or divide planes within a 3D model. This can be used to create planar geometric bodies, or reference planes can be used to split the model into parts for specific operations or analyses. In this adaptive modeling method, the reference planes are several larger base planes generated on the side, as illustrated in the Fig. 8. Within this framework, the 3D model is partitioned into distinct slices, with the blue segments representing the resultant 2D sketch profiles. Greater precision in subsequent lofting outcomes and closer conformance of resulting holes to the curved surface shape are achieved with a higher number of slices. However, increasing the number of slices means generating more sketches, which extends the program's runtime and reduces computational efficiency. Typically, selecting a range of 5–10 slices is deemed suitable for practical applications.

The development process commences with importing an editable curved surface model. Subsequently, the direction of extrusion surface and infill generation are selected. Parameters such as sandwich height H, print line width t, seam cutting width S, and number of slices m are inputted into the model. For trapezoidal infill, the chamfer radius r can be specified. The comprehensive algorithm flowchart is depicted in the Fig. 9.

The Fig.10. illustrates the automated modeling process for both the EPP and ECP of the triangular sandwich structure. Operation 1 involves importing an irregular curved surface. In Operation 2, the surface is projected onto a normal reference plane prior to extrusion, with the height H defined as the distance from the surface to the reference plane. Extrusion is then executed using the "offset from surface" command in SolidWorks. Operation 3 comprises loft cutting, which automatically generates the parameterized corrugated sandwich structure. Operation 4 involves seam cutting, where the model's paths are planned based on either the EPP path or ECP.

The pseudocode for some of the core algorithms is shown in the Table 1. During sketch construction, it is common to encounter issues with non-closed polygons such as triangles, trapezoids, and rectangles due to calculation precision problems. To address this, the clipping method is employed in this work. Initially, the *long_line* function is used to draw the extended lines of each edge in both directions. Subsequently, each extraneous edge is clipped to form a closed polygon as shown in the

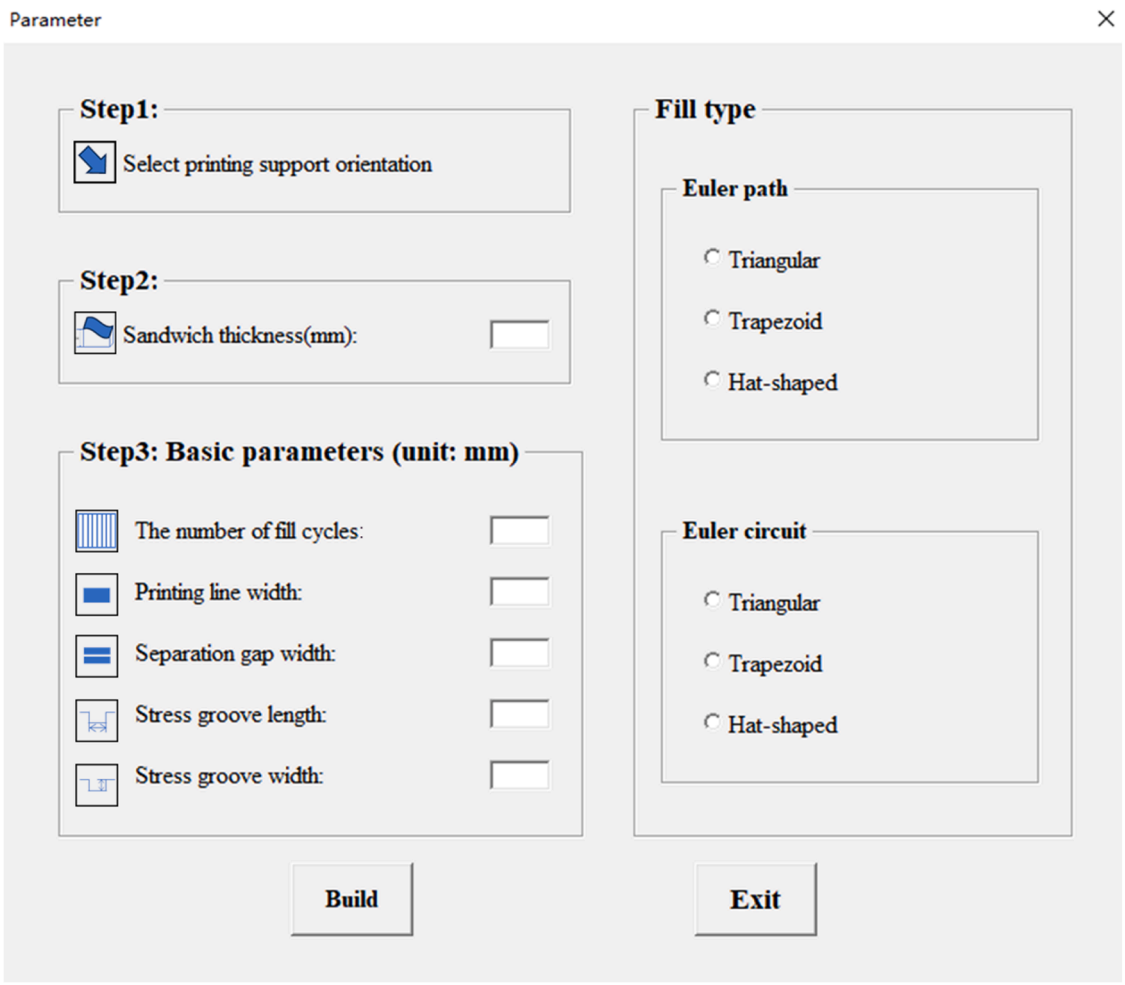


Fig. 12. Visualization interface for sandwich structure generation.

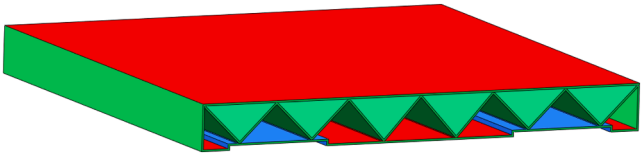


Fig. 13. The corrugated sandwich structure with stress grooves.

Fig. 11. Finally, the closed shapes on each slice sketch are selected and loft cuts are performed along 3D guide curves to generate the desired layers.

GUI development primarily involves three key components: registration files, user parameter input interface files, and core algorithm execution files. The registration file initiates the plug-in program, the user parameter input interface file defines parameters for the curved corrugated sandwich structure, and the core algorithm execution file executes automated modeling.

The GUI plug-in, depicted in the Fig. 12, outlines the following steps: Step 1 determines the direction of infill generation, typically chosen from two lateral directions. Step 2 allows users to input the filling height H based on specific requirements. Step 3 facilitates input for five parameters: the number of sandwich cycles m, print line width t, print seam width s, stress slot lengths$_l$, and stress slot widths$_w$.The optional printing module on the right side of the Fig. 12 categorizes methods into EPP and ECP. Each module includes triangular, trapezoid, and cap-shaped filling modes, each with distinct advantages and suitability for various practical engineering conditions.

When printing large-scale corrugated sandwich structures, the bottom plate of the printed part often deforms due to significant stress, resulting in an uneven bottom surface. Therefore, this paper proposes reducing the deformation of the bottom part of the sandwich structure by creating two large stress-relief grooves on the ground, as shown in the Fig. 13. Due to the stress relief grooves at the bottom, the height of the corrugated filling varies with the changes in the stress relief grooves of the bottom plate.

Different curved corrugated sandwich structures, due to the differences in the structure of the core material, have different modeling parameters for different problem structures, hence the relative density of the fill also varies. The relative density $\overline{\rho}$ of different corrugated core materials is shown in the Table 2, where m is the number of sandwich cycles, t is the line width, w is the width of the corrugated sandwich structure, h_s is the height of the curved panel, and l is the length of each cycle, which can be derived through Eq. (1):

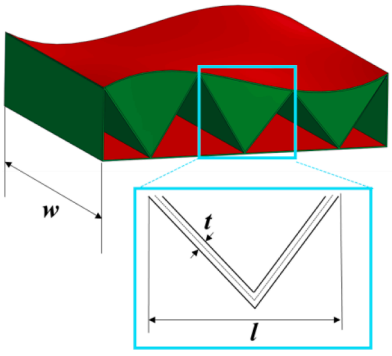
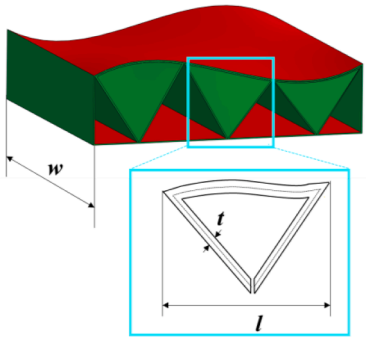
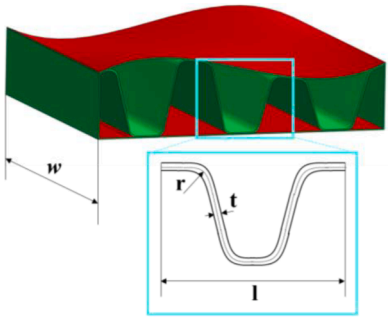
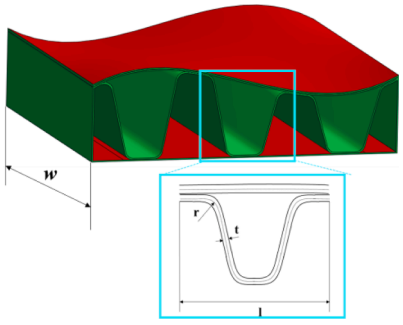
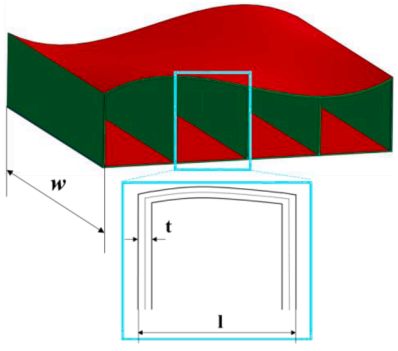
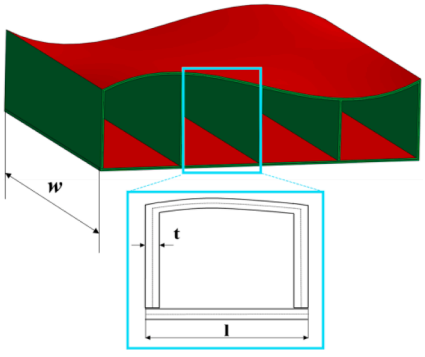
$$l = \frac{L}{m} \tag{1}$$

L represents the total length of the curved corrugated sandwich structure. It can be observed from the Table 2 that the relative density of the ECP, due to the presence of an additional path, is greater than the relative density of the EPP.

To ascertain the universality of adaptive automatic modeling, a diverse array of surfaces shall be employed. As shown in Fig. 14, encompassing planes, undulating surfaces, and intricate spatial surfaces. Different surfaces can be applied to different engineering applications.

Initially, a sandwich height of 200 mm was employed for the plane,

Table 2
The relative density of six types of corrugated sandwich structures.

EPP	ECP
	
$\bar{\rho} = \frac{\sum_1^m 2 \times t \times w \times \sqrt{\left(\frac{l}{2}\right)^2 + {h_m}^2} + 2 \times t \times h \times w}{\int\int_s h_s dS}$	$\bar{\rho} = \frac{\sum_1^m \left(2 \times t \times w \times \sqrt{\left(\frac{l}{2}\right)^2 + {h_m}^2} + \int_{l_m} t \times w dl\right) + 2 \times t \times h \times w}{\int\int_s h_s dS}$
	
$\bar{\rho} = \frac{\sum_1^m (2 \times t \times w \times l_m) + 2 \times t \times h \times w}{\int\int_s h_s dS}$	$\bar{\rho} = \frac{\sum_1^m \left(2 \times t \times w \times l_m + \int_{l_m} t \times w dl\right) + 2 \times t \times h \times w}{\int\int_s h_s dS}$
	
$\bar{\rho} = \frac{\sum_1^{m+1} \left(2 \times t \times w \times h_m + \int_{l_m} t \times w dl\right) + 2 \times t \times h \times w}{\int\int_s h_s dS}$	$\bar{\rho} = \frac{\sum_1^m \left(2 \times t \times w \times l_m + t \times w \times l + \int_{l_m} t \times w dl\right) + 2 \times t \times h \times w}{\int\int_s h_s dS}$

the number of support layer cycles is 6, featuring an 8 mm printing line width, 5 slicing iterations, and a 0.05 mm cut seam width to facilitate the modeling of six distinct models. Owing to the plane's notable regularity, extensive slicing for lofting and removal was deemed unnecessary. The resulting models derived from the six automated modeling methodologies are depicted in the accompanying Fig. 15.

Secondly, for the undulating surface, a sandwich height of 150 mm was selected, the number of support layer cycles is 6, with a printing line width of 4 mm, 7 slicing iterations, and a 0.05 mm cut seam width for the adaptive modeling of six models. As depicted in the Fig. 16, the sandwich height varies proportionally with the distance from the undulating surface to the base, ranging from 185 mm at its peak to 115 mm at its nadir.

Finally, concerning the intricate spatial surface, a sandwich height of 100 mm was stipulated, comprising 8 sandwich cycles, with a printing line width of 4 mm, 9 slicing iterations, and a 0.05 mm cut seam width for the automated modeling of six variants. As depicted in the Fig. 17, due to the variable nature of the sandwich height across different spatial positions within the complex surface, the height of the infill structure must also adjust correspondingly to the sandwich height.

Integrating the three types of automatic modeling corrugated sandwich structures mentioned earlier, based on the characteristics of ECP, the ECP model printing has an additional panel compared to the EPP model. The triangular filling and trapezoidal filling are mostly on the

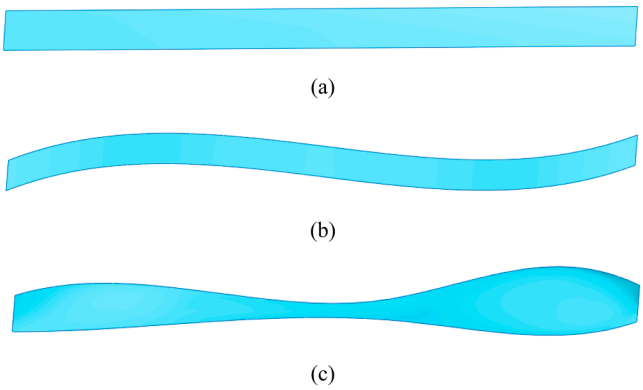


Fig. 14. Three surfaces for automated modeling: (a) Plane (b) Undulating surfaces (c) Intricate spatial surfaces.

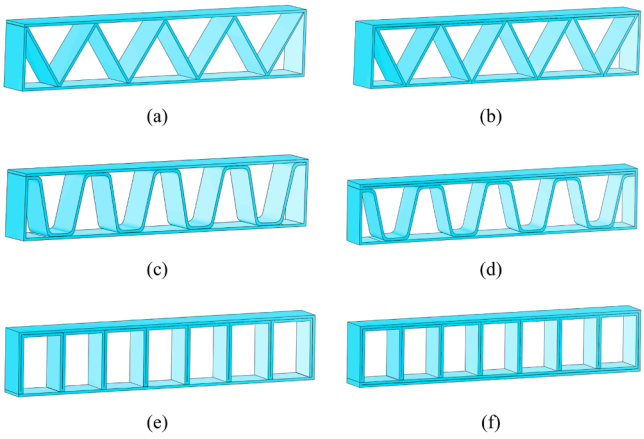


Fig. 15. Six types of adaptively generated plane models: (a) Triangular EPP infill (b) Triangular ECP infill (c) Trapezoidal EPP infill (d) Trapezoidal ECP infill (e) Cap-shaped EPP infill (f) Cap-shaped ECP infill.

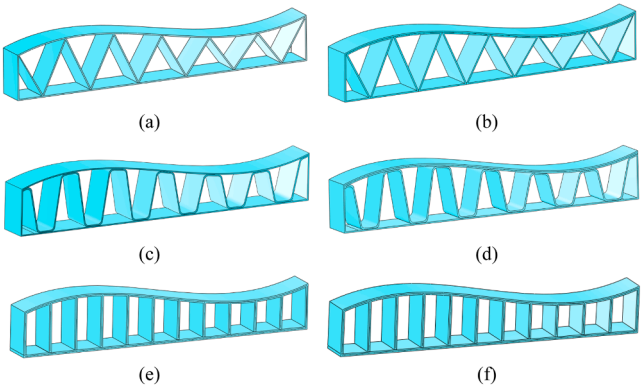


Fig. 16. Six types of adaptively generated undulating surfaces models: (a) Triangular EPP infill (b) Triangular ECP infill (c) Trapezoidal EPP infill (d) Trapezoidal ECP infill (e) Cap-shaped EPP infill (f) Cap-shaped ECP infill.

upper curved panel, while the cap-shaped filling is mostly on the lower flat panel. It is precisely because of this additional panel that the strength of the corrugated sandwich structure is enhanced. Different sandwich filling heights and different numbers of sandwich support cycles will lead to different support angles for the triangular and trapezoidal shapes.

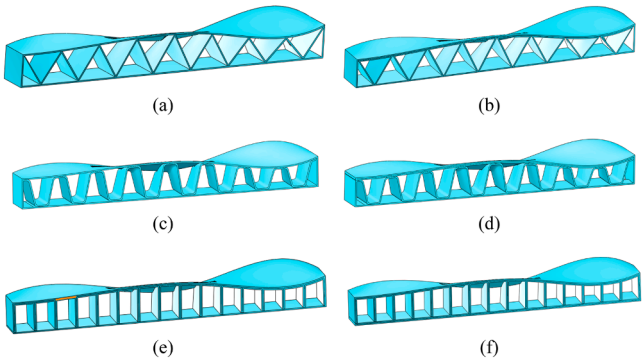


Fig. 17. Six types of adaptively generated intricate spatial surface models: (a) Triangular EPP infill (b) Triangular ECP infill (c) Trapezoidal EPP infill (d) Trapezoidal ECP infill (e) Cap-shaped EPP infill (f) Cap-shaped ECP infill.

4. Experimental methods and analysis

4.1. Print time analysis

In practical 3D printing applications, the duration of printing sessions holds significant relevance, particularly when fabricating large-scale objects, as it necessitates increased time and material resources. Consequently, the establishment of an optimal printing trajectory emerges as a crucial deliberation. Within the context of lightweight sandwich structures, the adoption of a judicious printing path can notably mitigate print duration while concurrently enhancing output quality.

To validate the feasibility of this study, a 3D printing process preview will be conducted using Ultimaker Cura for six types of pathway structures, implemented on both planar and undulating surfaces. The analysis will focus on evaluating printing time and material consumption. The Ultimaker S7 printer will be utilized, employing PLA material at 100 % infill density for simulation and emulation purposes.

In order to demonstrate the benefits of model path planning preprocessing, six models without path planning will also be developed. Specifically, these models will not undergo the preprocessing seam cutting operations of EPP and ECP, and the paths will be directly generated by the slicing software for printing.

In a selected flat corrugated sandwich structure with a 4-cycle filling configuration, the printing times for EPP and ECP are depicted in the Fig. 18, where the blue box represents the core relative density. The results illustrate that both EPP and ECP significantly reduce printing time compared to structures without seam cutting preprocessing.

During EPP method, a 1-minute idle travel occurs after each layer is printed, where the nozzle moves from the endpoint back to the starting point. Notably, no idle travel takes place during the layer printing process. The relative filling densities for the three types of EPP configurations are 4.3 %, 5.3 %, and 5.8 % respectively. Higher filling densities correlate with increased printing times and longer idle travel durations, with cap-shaped filling exhibiting the longest idle travel time of 4 min under normal printing conditions.

Notably, ECP method eliminates idle travel entirely, effectively preventing stringing phenomena during printing. The relative densities for the three ECP configurations are 6.2 %, 7.1 %, and 7.7 % respectively. Although the triangular ECP configuration demonstrates higher relative density compared to EPP configurations that without seam cutting preprocessing, it achieves a shorter printing time of 23 min, which is less than the time required for cap-shaped filling at 5.8 % relative density. Therefore, structures with higher filling densities benefit from reduced printing times when utilizing ECP configurations.

To facilitate a more comprehensive comparison of printing times, different filling cycles will be employed for modeling corrugated sandwich structures on undulating surfaces. Specifically, triangular filling

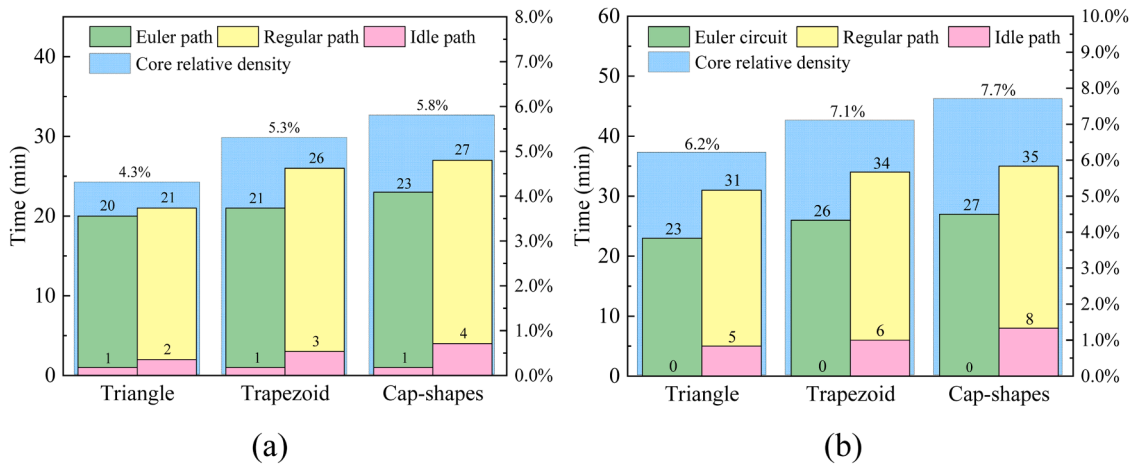


Fig. 18. The printing total time, idle travel time, and relative filling density of a corrugated sandwich structure with 4 filling cycles: (a) EPP (b) ECP.

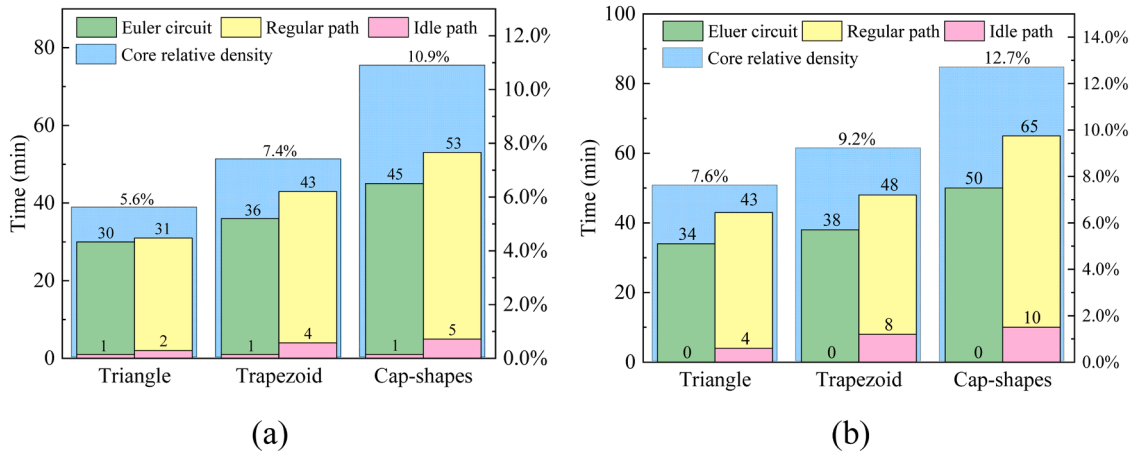


Fig. 19. The printing total time, idle travel time, and relative filling density of corrugated sandwich structures with different filling cycles: (a) EPP (b) ECP.

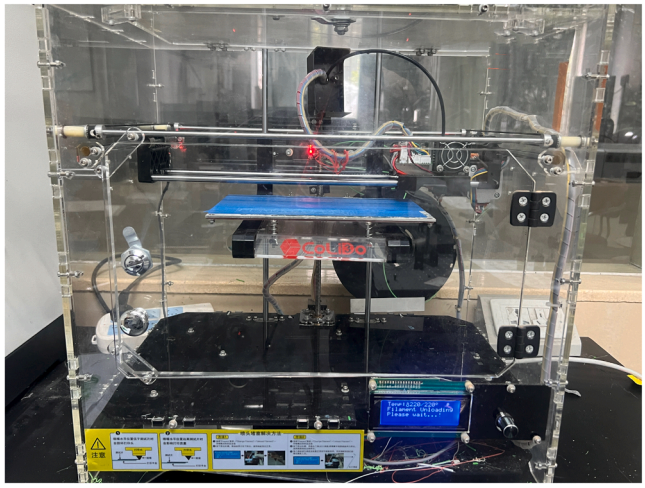


Fig. 20. CoLiDo 3D printer.

will utilize a 6-cycle, trapezoidal filling a 7-cycle, and cap-shaped filling an 11-cycle approach. The relative filling densities for EPP configurations are 5.6 %, 7.8 %, and 10.9 % respectively, while for ECP they are 7.6 %, 9.2 %, and 12.7 %. The corresponding printing times are illustrated in the Fig. 19.

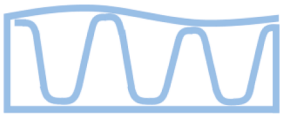
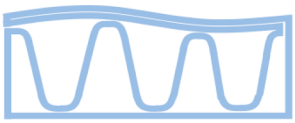
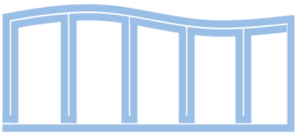
Notably, even with a 12.7 % filling density, the corrugated sandwich structure printed using the ECP under cap-shaped filling requires less time than EPP configurations that without seam cutting preprocessing at 10.9 % filling density. This efficiency is attributed to the ECP model's elimination of idle time and travel. Conversely, EPP configurations consistently incur a 1-minute idle travel time, which can adversely affect print quality due to material flow issues during nozzle heating and molten state.

Stringing issues, a common concern during prolonged idle travel, typically necessitate retraction as a mitigation strategy. However, managing retraction distance and speed is often labor-intensive and time-consuming. Therefore, preliminary path planning of the 3D model helps prevent stringing issues, optimizing material usage and enhancing overall printing efficiency.

4.2. *Experimental sample printing and testing methods*

This paper investigates the efficiency of a path planning method for printing curved sandwich structures compared to traditional approaches, emphasizing the need to assess its impact on mechanical properties. A corrugated curved model was utilized to explore six adaptive path planning schemes for 3D printing. The sandwich structure's height was fixed at 15 mm, incorporating triangular and trapezoidal fillings with a support cycle of 6. Additionally, a cap-shaped filling was tested with 11 cycles to evaluate mechanical properties under higher support loads. Parameters included a printing line width of 0.4

Table 3
Printed objects for six types of paths.

	Printing Path routes	Printed Objects
Triangle EPP		
Triangle ECP		
Trapezoid EPP		
Trapezoid ECP		
Cap-shaped EPP		
Cap-shaped ECP		

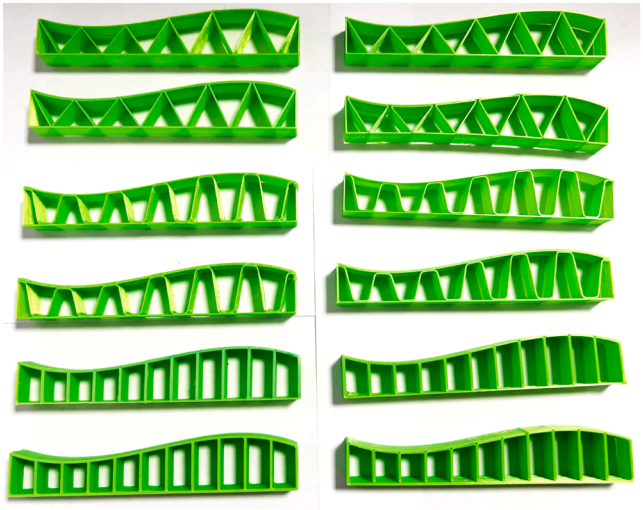


Fig. 21. On the left are the printed object images without path planning, and on the right are the printed object images with path planning.

mm and a seam cutting width of 0.05 mm. The corrugated surface ranged from 12 mm to 18 mm in height, measured from the bottom layer of the sandwich.

Export the G-code file using Ultimaker Cura and proceed with printing on a CoLiDo 3D printer, as illustrated in the accompanying Fig. 20. Common FDM printing materials include PLA, ABS, and PETG, among which PLA is widely used in various studies and experiments due to its ease of printing, biodegradability, and environmental friendliness.

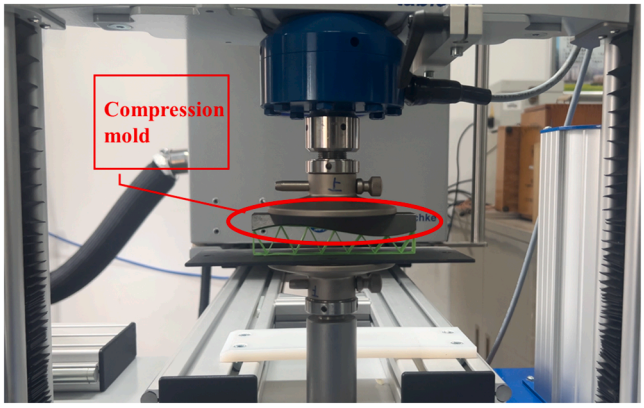


Fig. 22. Hegewald & Peschke testing apparatus.

In this study, PLA was selected as the test printing material. Its recommended print bed temperature ranges from 50 to 60 °C, while the nozzle temperature ranges from 180 to 220 °C. Considering the bonding characteristics of PLA, the material needs to be heated to a proper molten state to achieve suitable flowability, thereby enhancing inter-material contact and bonding. Consequently, the print bed temperature was set to 60 °C, and the nozzle temperature was set to 220 °C.The models involved in the experiment include six automatically generated objects, with their corresponding path schematic diagrams presented in Table 3.

To mitigate experimental variability, each model was printed in triplicate, resulting in a total of 18 pieces for the self-adaptive modeling

Table 4
The quality of specimen of various structural types.

	Printing method	Specimen mass (g)
Triangle	Euler path	4.12
	Regular path	4.29
	Euler circuit	5.03
	Regular path	5.23
Trapezoid	Euler path	4.72
	Regular path	4.92
	Euler circuit	5.49
	Regular path	5.85
Cap-shaped	Euler path	6.25
	Regular path	6.59
	Euler circuit	7.14
	Regular path	7.59

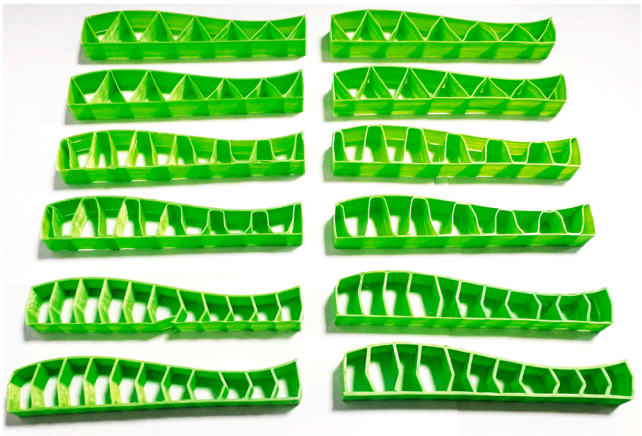


Fig. 23. Core shear failures of the Curved sandwich structure specimens.

models. The control group underwent no path planning during modeling; thus, G-code models were directly generated using Ultimaker Cura for 3D printing, also with three pieces printed for each type, totaling 18 pieces. Both sets of printed objects are depicted in the Fig. 21: the 6 objects on the left were printed under traditional conditions, while the 6 objects on the right underwent model path planning. Visual inspection reveals no significant macroscopic differences between the printed objects with varying printing paths.

The compression experiment of the curved wavy sandwich structure was conducted utilizing a Hegewald & Peschke testing apparatus. Given the undulating curvature of its upper surface, a bespoke compression mold conforming to this morphology is indispensable to ensure precise and replicable experimentation, as delineated in the Fig. 22. The compression procedure employs a controlled descent rate of 2 mm/min for the compression head. Each distinct compression sample variant will undergo a triad of trials to procure dependable data and fortify the veracity of the outcomes.

4.3. Experimental results and discussion

During experimental testing, it was noted that the utilization of EPP and ECP for modeling 3D printed curved sandwich structures exhibited no statistically significant deviation in their physical properties in contrast to those directly modeled for 3D printing. Nevertheless, a noteworthy reduction in printing time and a more efficient material consumption were achieved. The qualitative assessment of various 3D printed specimens, as depicted in the Table 4. Printed specimens that have undergone EPP and ECC exhibit a reduction in material usage by 3 % to 7 % compared to those printed without model preprocessing. Therefore, in practical engineering applications, preprocessing the model can save more printing time. Due to significant differences in the mass of the specimens, this variable is considered to have an impact on the overall mechanical performance.

Following the compression test, deformation manifested within the core material of the structure, as depicted in the Fig. 23, signaling localized failure in these sandwich structures. Subsequent analysis reveals that the primary mechanism underlying structural failure is attributed to the shearing of the sandwich core material. Given that the principal load-bearing forces acting upon the sandwich structure are predominantly vertical in nature, the integrity of the surface structure remains largely intact, with localized failures primarily concentrated within the core material of the sandwich.

In experimental investigations, sandwich structures are frequently delineated through load-displacement diagrams, offering a lucid portrayal of their mechanical attributes. During compression testing, samples exhibiting anomalous data were omitted, and the remaining samples underwent mean processing to derive the load-displacement curve specific to the curved sandwich structure under compression, as depicted in the Fig. 24. Notably, examination of the load-displacement curves derived from the 12 distinct sample types (comprising six subjected to path planning and six without) reveals uniform trends: preceding shear failure, the load-displacement relationship exhibits a predominantly linear trajectory, however, upon the onset of shear failure, there is an abrupt decline in structural load-bearing capacity. It is commonly observed that shear failure tends to manifest proximate to the region where the compression head descends by approximately 1 mm.

The curved sandwich structures featuring triangular core, fabricated through the utilization of EPP and ECP, demonstrate enhanced mechanical efficacy compared to their conventionally directly printed counterparts. The average maximum load-bearing capacity of each specimen, as delineated in the Table 5. Specifically, the triangular infill structures exhibit a notable augmentation in maximum load-bearing capacity, with the EPP and ECP specimens manifesting increments of 6.8 % and 10.5 %, respectively, over traditional printing methodologies.

Conversely, the wavy infill structures exhibit a marginal decrement in maximum load-bearing capacity when compared to traditional printing techniques. The EPP and ECP specimens reflect reductions of 5.8 % and 6.6 %, respectively, as detailed in the Table 6. Notably, within the cap-shaped infill structures, the EPP specimens exhibit a slight inferiority in performance relative to traditional printing approaches. However, in the cap-shaped filling structure, the specimens printed with the EPP showed a 5.0 % increase in maximum load-bearing capacity compared to traditional printing, while the ECP experienced a 2.0 % reduction, as indicated in the Table 7.

In summary, while the specimens fabricated utilizing EPP and ECP methodologies experience slight reductions in maximum load-bearing capacity in certain scenarios, such differences remain within a 10 % margin. Overall, these approaches do not significantly compromise the mechanical efficacy of the curved sandwich structures.

Upon comparison of the aforementioned data, it becomes evident that the specimens fabricated using EPP and ECP exhibit comparable mechanical properties to those printed via traditional methods. However, when considering printing duration and material utilization, the implementation of EPP and ECP methodologies entails preemptive path planning during the model's preprocessing phase, leading to a significant reduction in idle traversal time during the printing process. Consequently, this approach yields substantial time savings in printing while concurrently enhancing the fidelity of the resultant printed objects. Notably, for voluminous printed structures, the efficiency gains are particularly pronounced. It is noteworthy that the ECP method can even obviate the necessity for idle traversal altogether during the printing process, thereby further optimizing both printing efficiency and output quality.

From an alternative perspective concerning filling geometry, the curved sandwich structure incorporating cap-shaped infill materializes as superior in its mechanical response to compression load-bearing. Conversely, while the wavy filling marginally surpasses triangular

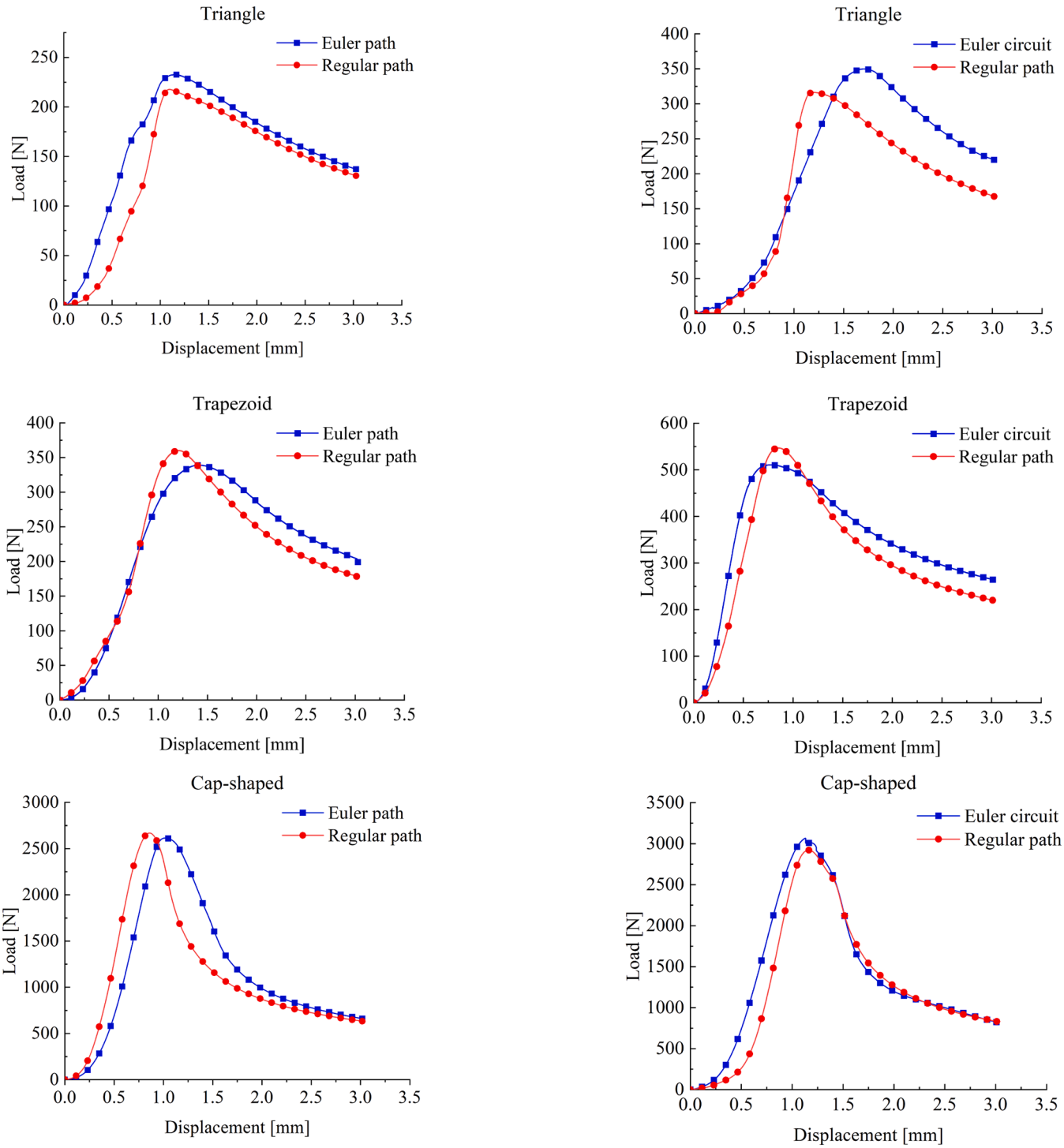


Fig. 24. Displacement-Load curve from the compression test of curved sandwich structures.

Table 5
Triangle fill different types of printing methods maximum support load.

Triangle	Maximum load (N)
EPP	232.75
Regular path	217.87
ECP	349.91
Regular path	316.41

Table 6
Trapezoid fill different types of printing methods maximum support load.

Trapezoid	Maximum load (N)
EPP	339.10
Regular path	359.96
ECP	510.72
Regular path	546.89

Table 7
Hat-shaped fill different types of printing methods maximum support load.

Cap-shaped	Maximum load (N)
EPP	2614.77
Regular path	2668.45
ECP	3067.15
Regular path	2921.83

filling in compression load-bearing performance, it significantly lags behind the efficacy of the cap-shaped configuration, delineating a disparity of approximately tenfold. This discrepancy stems from the predominant mechanical orientation observed in compression testing, primarily directed vertically. Notably, the structural alignment of the cap-shaped infill correlates with the force direction, thereby optimizing its capacity to endure compressive forces effectively.

5. Conclusion

This study is grounded in the secondary development of SolidWorks and presents an innovative automatic adaptive modeling interface plug-in tailored for curved corrugated sandwich structures. Through automated parameterization and swift modeling of planes, undulating surfaces, and intricate spatial surfaces, it alleviates the burden of laborious modeling tasks while enhancing modeling efficiency. Moreover, empirical validation demonstrates the plug-in interface's compatibility with diverse complex and irregular surface conditions. Additionally, two novel model preprocessing techniques, namely EPP and ECP, are introduced to mitigate idle travel during printing. Particularly, the ECP printing method, characterized by zero idle travel, mitigates the risk of filament dragging on printed parts, thus elevating print quality. The automatic modeling of path planning for corrugated sandwich structures in 3D printing has been evaluated in comparison to traditional printing methods in terms of printing time and material consumption. The results demonstrate significant improvements in printing efficiency and cost savings, offering broad application prospects in aerospace, construction, and related fields. However, when applied to these highly regulated industries, challenges inherent to 3D printing, such as printing accuracy, process integration, and structural strength consistency, still need to be addressed through further research and advancements. Furthermore, mechanical properties of the printed method are validated through compression experiments. The observed maximum load-bearing difference between 3D printed parts utilizing the proposed path planning method and traditional 3D printing falls within 10 %, suggesting that the mechanical properties of curved corrugated sandwich structures are predominantly governed by their intrinsic structure rather than the printing path.

Presently, the developed automatic modeling plug-in caters to a singular type of corrugated sandwich structure. Future endeavors will leverage this research foundation to further refine automatic adaptive modeling methodologies for diverse filling techniques such as honeycomb, diamond, and auxetic structures. Additionally, expansion towards accommodating various model surfaces, including cylindrical and spherical surfaces, will facilitate the automatic generation of corresponding sandwich structures.

CRediT authorship contribution statement

Tan Gui: Writing – review & editing, Writing – original draft, Software, Methodology, Investigation. **Zhihong Li:** Supervision, Resources, Conceptualization. **Yongjun Cao:** Software, Methodology. **Jianghong Yang:** Software, Methodology. **Yingjun Wang:** Writing – review & editing, Supervision, Funding acquisition, Conceptualization.

Declaration of competing interest

The authors declare that they have no known competing financial interests or personal relationships that could have appeared to influence the work reported in this paper.

Acknowledgment

This work has been supported by Guangdong Basic and Applied Basic Research Foundation [No. 2024A1515011786], National Natural Science Foundation of China [No. 52075184]. These supports are gratefully acknowledged.

Data availability

Data will be made available on request.

References

[1] L.J. Gibson, M.F. Ashby, Cellular Solids: Structure and Properties, 2 ed, Cambridge University Press, Cambridge, 1997.
[2] D. Zenkert, N.I. Fund, The Handbook of Sandwich Construction: Engineering Materials Advisory Services (1997).
[3] C. Shen, F.X. Xin, T.J. Lu, Theoretical model for sound transmission through finite sandwich structures with corrugated core, Int. J. Non. Linear. Mech. 47 (2012) 1066–1072.
[4] F. Mesquita, A. van Gysel, M. Selezneva, Y. Swolfs, S.V. Lomov, L. Gorbatikh, Flexural behaviour of corrugated panels of self-reinforced polypropylene hybridised with carbon fibre: an experimental and modelling study, Composites Part B: Engineering 153 (2018) 437–444.
[5] M.R.M. Rejab, W.J. Cantwell, The mechanical behaviour of corrugated-core sandwich panels, Compos. Part B Eng. 47 (2013) 267–277.
[6] K. Zhang, Y. Hou, Y. Lu, J. Ke, Y. Ke, W. Yang, Parametric modeling and mechanical investigation of an aluminum-bamboo corrugated sandwich structure, Structures 62 (2024) 106138.
[7] Q. Zhang, X. Yang, P. Li, G. Huang, S. Feng, C. Shen, et al., Bioinspired engineering of honeycomb structure – Using nature to inspire human innovation, Prog. Mater. Sci. 74 (2015) 332–400.
[8] B.L. Buitrago, C. Santiuste, S. Sánchez-Sáez, E. Barbero, C. Navarro, Modelling of composite sandwich structures with honeycomb core subjected to high-velocity impact, Compos. Struct. 92 (2010) 2090–2096.
[9] L. Valdevit, J.W. Hutchinson, A.G. Evans, Structurally optimized sandwich panels with prismatic cores, Int. J. Solids. Struct. 41 (2004) 5105–5124.
[10] X. Zhu, C. Xiong, J. Yin, H. Zhou, Y. Zou, Z. Fan, et al., Experimental study and modeling analysis of planar compression of composite corrugated, lattice and honeycomb sandwich plates, Compos. Struct. 308 (2023) 116690.
[11] T.A. Schaedler, W.B. Carter, Architected Cellular Materials, Annu Rev. Mater. Res. 46 (2016) 187–210.
[12] B. Castanie, C. Bouvet, M. Ginot, Review of composite sandwich structure in aeronautic applications, Compos. Part C Open Access 1 (2020) 100004.
[13] P.R. Oliveira, M. May, T.H. Panzera, S. Hiermaier, Bio-based/green sandwich structures: a review, Thin-Walled Struct. 177 (2022) 109426.
[14] J.J. Rimoli, B. Talamini, J.J. Wetzel, K.P. Dharmasena, R. Radovitzky, H.N. G. Wadley, Wet-sand impulse loading of metallic plates and corrugated core sandwich panels, Int. J. Impact. Eng. 38 (2011) 837–848.
[15] H.N.G. Wadley, Multifunctional periodic cellular metals, Philosoph. Trans. Royal Soc. A Math. Phys. Eng. Sci. 364 (2006) 31–68.
[16] S. Rossi, A. Puglisi, M. Benaglia, Additive Manufacturing Technologies: 3D printing in organic synthesis, ChemCatChem. 10 (2018) 1512–1525.
[17] E.O. Olakanmi, R.F. Cochrane, K.W. Dalgarno, A review on selective laser sintering/melting (SLS/SLM) of aluminium alloy powders: processing, microstructure, and properties, Prog. Mater. Sci. 74 (2015) 401–477.
[18] K. Singh, Experimental study to prevent the warping of 3D models in fused deposition modeling, International Journal of Plastics Technology 22 (2018) 177–184.
[19] M. Benamira, N. Benhassine, A. Ayad, A. Dekhane, Investigation of printing parameters effects on mechanical and failure properties of 3D printed PLA, Eng. Fail. Anal. 148 (2023) 107218.
[20] W. Han, M.A. Jafari, S.C. Danforth, A. Safari, Tool path-based deposition planning in fused deposition processes, J. Manuf. Sci. Eng. 124 (2002) 462–472.
[21] C. Hauser, M. Dunschen, M. Egan, C. Sutcliffe, Transformation algorithms for image preparation in spiral growth manufacturing (SGM), Rapid. Prototyp. J. 14 (2008) 188–196.
[22] K. Yamamoto, J.V.S. Luces, K. Shirasu, Y. Hoshikawa, T. Okabe, Y. Hirata, A novel single-stroke path planning algorithm for 3D printers using continuous carbon fiber reinforced thermoplastics, Addit. Manuf. 55 (2022) 102816.
[23] Y. Tu, Y. Tan, F. Zhang, J. Zhang, G. Ma, Shearing algorithm and device for the continuous carbon fiber 3D printing, Journal of Advanced Mechanical Design, Systems, and Manufacturing 13 (2019). JAMDSM0016-JAMDSM.

[24] S.R.G. Bates, I.R. Farrow, R.S. Trask, 3D printed polyurethane honeycombs for repeated tailored energy absorption, Mater. Des. 112 (2016) 172–183.
[25] Y. Chen, T. Li, Z. Jia, F. Scarpa, C.-W. Yao, L. Wang, 3D printed hierarchical honeycombs with shape integrity under large compressive deformations, Mater. Des. 137 (2018) 226–234.
[26] R. Rajpal, L. K.P, K.V Gangadharan, Parametric studies on bending stiffness and damping ratio of Sandwich structures, Addit. Manuf. 22 (2018) 583–591.
[27] S. Pirouzfar, A. Zeinedini, Effect of geometrical parameters on the flexural properties of sandwich structures with 3D-printed honeycomb core and E-glass/epoxy face-sheets, Structures 33 (2021) 2724–2738.
[28] S. Kang, W. Liu, J. Wang, H. Song, W. Yuan, C. Huang, Self-adaptive 3D lattice for curved sandwich structures, Addit. Manuf. 54 (2022) 102761.
[29] D. Zhao, T. Liu, X. Lu, X. Meng, Experimental and numerical analysis of a novel curved sandwich panel with pultruded GFRP strip core, Compos. Struct. 288 (2022) 115404.
[30] C. Liu, C. Ma, X. Gao, Study on impact behavior of glass fiber/PVC curved sandwich structure composites, Polym. Compos. (2022).
[31] W. Hou, Y. Shen, K. Jiang, C. Wang, Study on mechanical properties of carbon fiber honeycomb curved sandwich structure and its application in engine hood, Compos. Struct. 286 (2022) 115302.
[32] S. Danjou, N. Lupa, P. Köhler, Approach for automated product modeling using knowledge-based design features, Comput. Aided. Des. Appl. 5 (2008) 622–629.
[33] M. Shaqura, J.S. Shamma, An automated quadcopter CAD based design and modeling platform using Solidworks API and Smart Dynamic Assembly, in: International Conference on Informatics in Control, Automation and Robotics, 2017.
[34] L. Yang, F. Shi, X. Sun, Y. Cheng, SolidWorks visualization of 3D fracture geometry in tight oil reservoirs, J. Therm. Anal. Calorim. 139 (2020) 2647–2657.
[35] Y. Jin, Y. He, J. Du, A novel path planning methodology for extrusion-based additive manufacturing of thin-walled parts, Int. J. Comput. Integr. Manuf. 30 (2017) 1301–1315.
[36] Y. Jin, Y. He, G. Fu, A. Zhang, J. Du, A non-retraction path planning approach for extrusion-based additive manufacturing, Robot. Comput. Integr. Manuf. 48 (2017) 132–144.
[37] B. Bollobás, Modern Graph Theory, Graduate Texts in Mathematics, 2002.
[38] F. Xia, T. Pang, G. Sun, D. Ruan, Longitudinal bending of corrugated sandwich panels with cores of various shapes, Thin-Walled Structures 173 (2022) 109001.
[39] T. Hagerup, F. Kammer, M. Laudahn, Space-efficient Euler partition and bipartite edge coloring, Theor. Comput. Sci. 754 (2019) 16–34.